Ore Geology Reviews 64 (2015) 747–755

Contents lists available at ScienceDirect

Ore Geology Reviews

journal homepage: www.elsevier.com/locate/oregeorev

Geochemical distribution and supergene behavior of indium at the Pingüino epithermal polymetallic vein system, Patagonia, Argentina

Luciano Lopez *, Sebastián M. Jovic, Diego M. Guido, Conrado Permuy Vidal, Gerardo N. Páez, Remigio Ruiz

Consejo Nacional de Investigaciones Científicas y Técnicas (CONICET), Instituto de Recursos Minerales (INREMI), Facultad de Ciencias Naturales y Museo, Universidad Nacional de La Plata, Paseo del Bosque s/n, B1900FWA, La Plata, Argentina

ARTICLE INFO

Article history:
Received 30 August 2013
Received in revised form 1 May 2014
Accepted 8 May 2014
Available online 28 May 2014

Keywords:
Indium
Critical metal
Supergene behavior
Oxidation zone
Mobility
Geochemistry
Deseado Massif
Argentina

ABSTRACT

The Pingüino deposit, located in the low sulfidation epithermal metallogenic province of the Deseado Massif, Patagonia, Argentina, represents a distinct deposit type for this region. It evolved through two different mineralization events: an early In-bearing polymetallic event that introduced In, Zn, Pb, Ag, Cd, Au, As, Cu, Sn, W and Bi, represented by a complex sulfide assemblage, and late Ag–Au quartz-rich veining that crosscut and overprinted the early polymetallic mineralization. Three In-bearing mineralization stages were identified within the polymetallic event. Iron-rich sphalerite of the second stage is the major In carrier in the deposit. The spatial distribution of In within the veins shows its maximum mean values in the Marta Centro and Ivonne Norte veins, in a pattern similar to the Zn distribution, showing a close spatial relation with the unexposed Kasia intrusive complex. At the vein scale, and in the hypogene zone, the In distribution is associated with variations in the temperature of mineralizing fluids. The vertical distribution of In within the veins exhibits consistent values both below and above the oxidation level, resembling the behavior of Pb and Sn, and therefore suggesting that In behaves as an immobile element during vein weathering.

1. Introduction

Indium is currently one of the crucial elements for a wide variety of high technology applications (e.g., solar cells, semiconductors, LCD screens, etc.; Dill et al., 2013), although most of this metal is recovered as a by-product during zinc-ore processing. It is also currently exploited from two primary sources: massive sulfide deposits (Schwarz-Schampera and Herzig, 2002) and tin-polymetallic-zinc deposits of vein and fissure-filling types (Murakami and Ishihara, 2013). Despite the current interest in the exploration for and study of, mineral deposits carrying this critical metal, relatively little is known about its geochemical behavior during crystallization of sulfide assemblages, weathering and mobilization of In-bearing ores.

The Deseado Massif is located in the Santa Cruz province, southern Patagonia, Argentina. Currently, this region is an important Au–Ag producer with four active mines (Cerro Vanguardia, San José, Manantial Espejo and Lomada de Leiva). Most of the Au–Ag mineralization occur within low sulfidation epithermal deposits that are spatially, temporally and genetically related to a complex and long-lived (>30 Ma) Middle to Upper Jurassic volcanic event associated with tectonic extension (Guido and Schalamuk, 2003).

In the past few years, the presence of indium has been reported in some epithermal deposits from Patagonia, including Pingüino (Guido et al., 2005; Jovic et al., 2011a) in the Deseado Massif, and La Luz (Trendix, 2006), San Roque (Dill et al., 2013; Gómez et al., 2008), Toruel (Marifil Mines Ltd., 2010) and Gonzalito (Gozalvez et al., 2008) in northern Patagonia. Within this framework, the Pingüino deposit is considered as an atypical deposit as its mineralogy and metal association deviate from the usual low sulfidation model of the Deseado Massif (Jovic et al., 2011a,b,c). The deposit is located in the central part of this region, 40 km to the northwest of the Au–Ag Cerro Vanguardia mine (Guido et al., 2005). Pingüino comprises >70 different veins, 16 of which show high-grade ore-shoots; eight of these ore-shoots contain 23.6 million ounces Ag eq., at an average grade of 132.4 g/t Ag eq. (modeling Ag, Au, Pb and Zn) as an indicated mineral resource estimate (Ristorcelli et al., 2013). The mineralization is characterized by the presence of two vein types, early polymetallic sulfide-rich veins (In–Zn–Pb–Ag–Au-bearing) and late quartz-rich veins (Au–Ag-bearing).

The presence and distribution of In in the Pingüino vein system was previously studied by Jovic (2010) and Jovic et al. (2011a,b), who mostly focused on the hypogene mineralization, with special emphasis on metal correlations and the distribution of In within different minerals.

* Corresponding author at: Instituto de Recursos Minerales, Calle 64 y Calle 120, La Plata 1900, Buenos Aires, Argentina. Tel./fax: +54 221 4225648.
E-mail address: lopezluciano@hotmail.com (L. Lopez).

http://dx.doi.org/10.1016/j.oregeorev.2014.05.010
0169-1368/

The aim of the present study is to analyze the distribution of In at the deposit scale, as well as the supergene geochemical behavior of this element in relation to polymetallic mineralization in an atypical epithermal system, and to provide insights on the mobility of this critical metal during weathering of polymetallic ores.

2. Geological setting of the Pingüino deposit

The Deseado Massif (Fig. 1) is a 60,000 km^2 geological region located in the southern part of Extra-Andean Patagonia, in the central part of the Santa Cruz province. During the Middle to Upper Jurassic, a volcanic mega-event occurred in Patagonia, giving rise to the Chon Aike Large Igneous Province (Pankhurst et al., 1998). In the Deseado Massif, this event is represented by a volcanic suite, known as the Bahía Laura Volcanic Complex (BLVC). Pyroclastic rocks predominate within the BLVC, with subordinate amounts of intercalated lavas of andesitic to rhyolithic composition. Intricate stratigraphic relationships characterize this complex, with multiple intercalations of different rock facies. The BLVC contains numerous gold and silver epithermal deposits, leading Schalamuk et al. (1999) to define the Deseado Massif as an Au–Ag metallogenic province. The majority of the Au–Ag occurrences are epithermal low sulfidation (LS) style (Echavarría et al., 2005; Fernández et al., 2008; Guido and Schalamuk, 2003), but in the past few years epithermal intermediate sulfidation (Martha mine, González Guillot et al., 2004; Páez et al., 2011) and polymetallic vein deposits (Pingüino Guido et al., 2005; Jovic, 2010) have also been reported.

The Pingüino deposit is located in the central part of the Deseado Massif (Fig. 1) and is characterized by the unique presence of pre-BLVC rocks. The sequence starts with Middle to Upper Triassic continental sedimentary rocks of El Tranquilo Group (Jalfin and Herbst, 1995; Fig. 2a), composed of fine to coarse sandstones with volcanic components, and a rhythmic alternation of siltstones, mudstones, black shales and coal strata. Dioritic intrusive bodies (mainly laccoliths), with associated basic to intermediate sills and dikes, assigned to the La Leona Formation of probably Lower Jurassic age (Jovic, 2010), intrude the Triassic sequence. Overlaying the previous units is the Lower Jurassic Roca Blanca Formation (Herbst, 1965), composed of epiclastic and pyroclastic fine-grained sandstones with intercalations of conglomerates and tuffaceous rocks and minor ignimbrite deposits. Basaltic lava flows of El Piche Formation (Jovic, 2010) occur in the northern part of the area, overlying and interbedded within the volcaniclastic rocks of the Roca Blanca Formation. Finally, toward the northwestern sector of the study area, the sequence was intruded by a series of andesitic subvolcanic bodies, assigned to the Middle Jurassic Cerro León Formation (Panza, 1995).

The El Tranquilo Fault (Fig. 2a) is a major brittle structure in the area, associated with a series of second-order extensional faults developed to the east (Jovic, 2010). The Pingüino vein system is composed of veins that infill these second-order structures with NNW, NW and ENE orientations and extend for a total length of 112 km. These veins crosscut the Triassic continental sedimentary rocks and the Lower Jurassic epiclastic and volcaniclastic rocks (Fig. 2a).

The mineralized area is located in the center of a regional dome structure, known as the El Tranquilo Anticline. This structural dome (15 to 20 km in diameter) is characterized by the presence of a series of radial faults, and was interpreted as a shallow-crust expression of an unexposed igneous body located below a depth of 1.5 km (Peñalva et al., 2008).

Local small-scale folding structures (domes, <2 km in diameter) are also recognized in the Pingüino area (Fig. 2b). These domes represent local deformation associated with generally non-outcropping subvolcanic bodies of dioritic (La Leona Formation) and minor andesitic (Cerro Leon Formation) compositions, that are located at depths between 80 and 200 m below the surface, and have been confirmed by regional and detailed magnetometric surveys (Fig. 2a), mine drilling and hydrocarbon exploration drilling (Cortiñas et al., 2005; Peñalva et al., 2008; Ristorcelli et al., 2013). These intrusions are clearly imaged in a magnetometric map (Fig. 2b) and are shown in a SW-NE geological cross-section in Fig. 3. Small faults, lacking a defined orientation, are concentrated around the local domes, and are interpreted to have probably been generated during the emplacement of these small subvolcanic bodies. They are

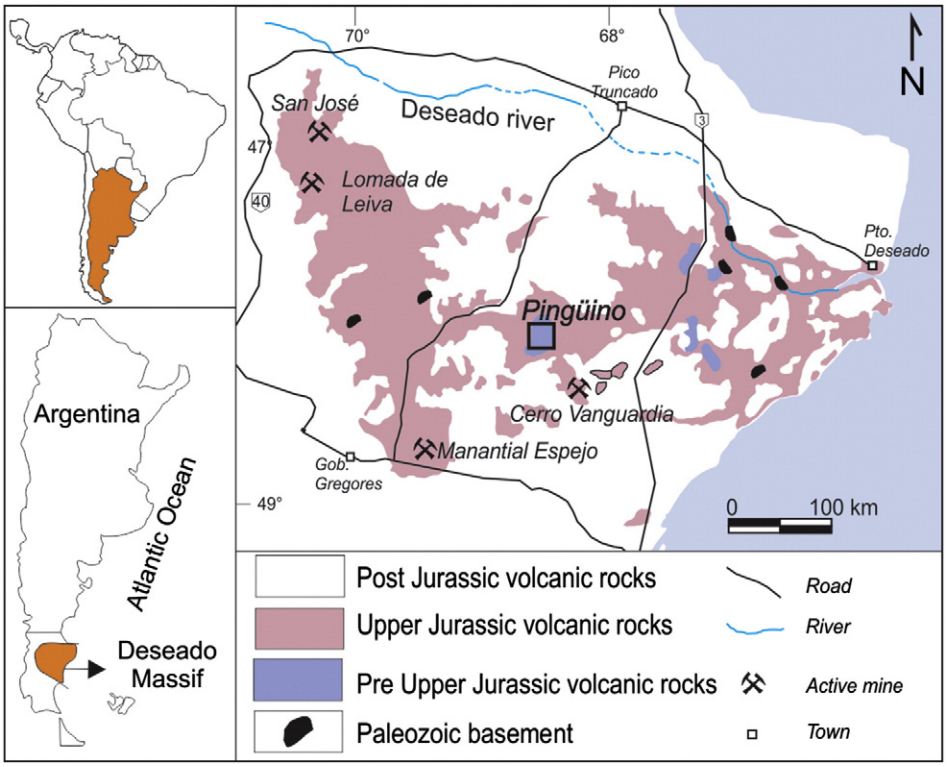

Fig. 1. Geological map of the Deseado Massif showing the location of the Pingüino deposit and the active mines.

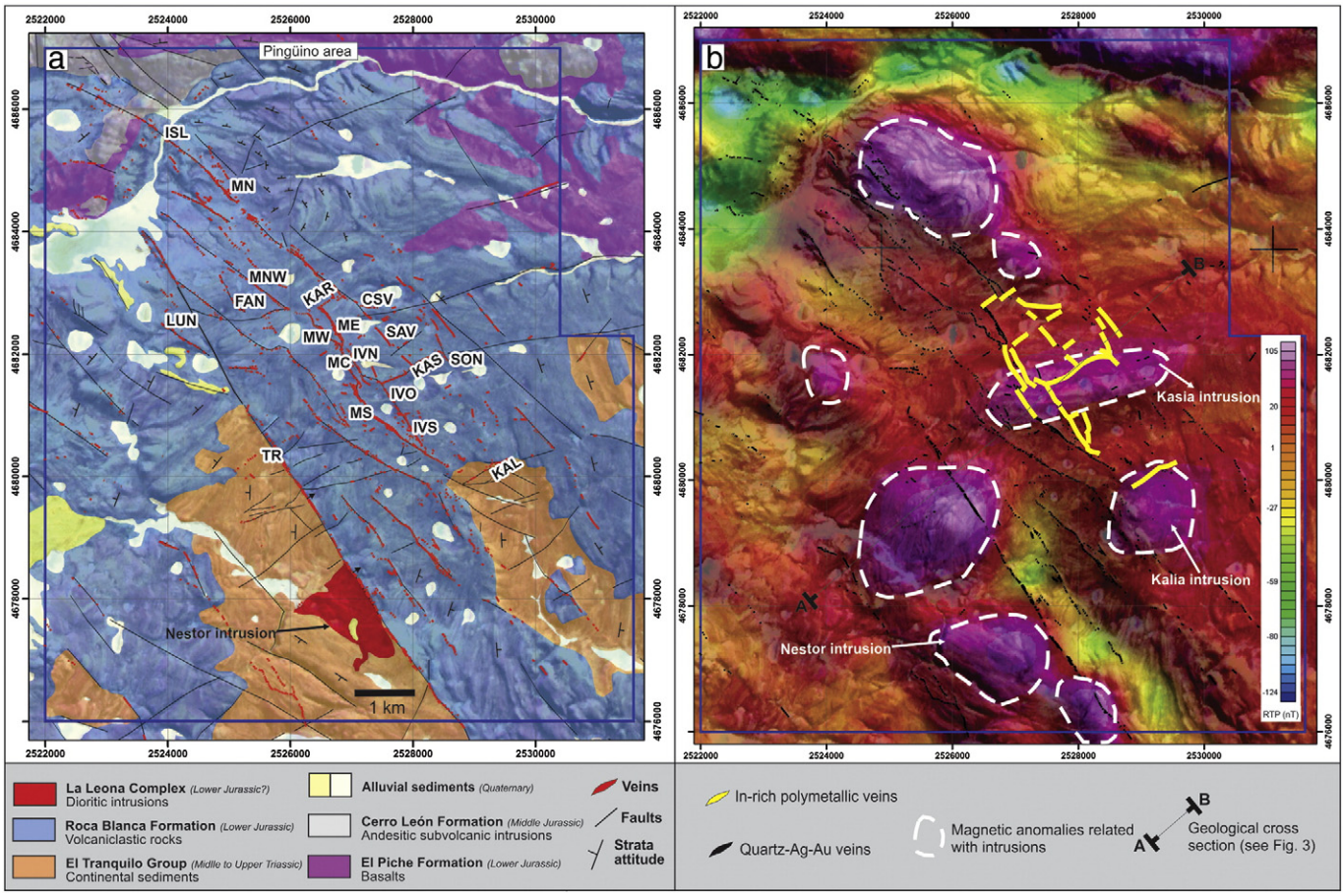

Fig. 2. a) Simplified geological map of the Pingüino deposit superimposed on a Landsat TM image. Veins' names are abbreviated as follows: ISL: Isla, MN: Marta Norte, MNW: Marta Noroeste, LUN: Luna, FAN: Fantasma, KAR: Karina, MW: Marta Oeste, ME: Marta Este, SAV: Savary, MC: Marta Centro, IVN: Ivonne Norte, MS: Marta Sur, IVO: Ivonne, KAS: Kasia, SON: Sonia, KAL: Kalia, and TR: Tranquilo. b) Regional magnetometric map superimposed on a Landsat TM image, showing the main anomalies (red–violet) in the total magnetic field reduced to pole (RTP in nT), these anomalies correspond to unexposed subvolcanic bodies. Note the spatial relation between the sulfide veins and the subvolcanic bodies (modified from Peñalva et al., 2008).

mainly sub-circular in shape, probably represent laccoliths, and are interpreted as shallow stocks, derived from the main intrusion related to the regional anticline. Commonly, these intrusions are aligned in a NNW-SSE direction, with the exception of a series of intrusions located in the central portion of the study area, where they constitute an ENE-WSW trend (Fig. 2b). Finally, there is a clear spatial relation between

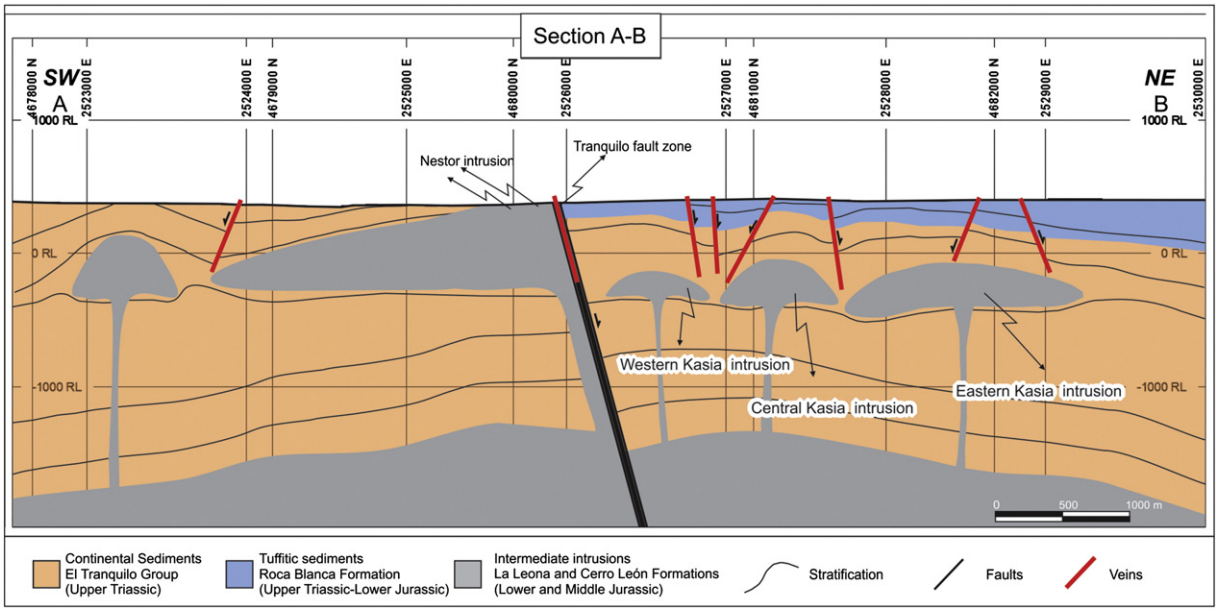

Fig. 3. Geological cross-section. See the location in Fig. 2b.

the intrusions and high-grade veins (Jovic, 2010), where most of the high-grade ore-shoots are located in faults dipping outwards from the roofs of the intrusions (Figs. 2b and 3).

3. Indium-bearing polymetallic mineralization

The Pingüino deposit represents a distinct deposit type in comparison with the well-known low sulfidation epithermal mineralization in the region (Jovic et al., 2011a). It has evolved through two different mineralization events. The first was an early In-bearing polymetallic event that introduced In, Zn, Pb, Ag, Cd, Au, As, Cu, Sn, W and Bi, represented by a complex sulfide assemblage, and located mainly along NNW-trending fractures (Tranquilo trend), and less commonly developed in ENE-trending fractures (Kasia trend). The second event is represented by late Ag–Au quartz-rich veins, hosted in NW-trending fractures (Marta trend), crosscutting and overprinting the early polymetallic mineralization, leading to the juxtaposition, in some cases, of the two different mineralization styles in the same fault system. The quartz-rich veins share similar characteristics with typical epithermal low to intermediate sulfidation deposits elsewhere in the Deseado Massif (Jovic, 2010) and will not be further discussed here.

The indium-bearing polymetallic mineralization was developed in three stages (Figs. 4 and 5; Jovic et al., 2011a,c): an early Cu–Au–As–Sn–In–W–Bi stage (Ps_1), characterized by complex ore mineralogy, mainly composed of idiomorphic pyrite crystals, zoned arsenopyrite crystals, hypidiomorphic crystals of chalcopyrite, Sn minerals (cassiterite, ferrokësterite and stannite), hübnerite and very fine-grained (<50 μm) acicular and prismatic Ag–Pb–Bi sulfosalts like aramayoite, owyheeite, ourayite, giessenite and izoklakeite. The second stage (Ps_2) is dominated by a Zn, Pb, Ag, In, Cd and Sb assemblage, where most Ps_1 minerals were brecciated and replaced by banded sphalerite and galena. Tetrahedrite, freibergite, argentotennantite, Pb–Ag sulfosalts and minor late crystallizing enargite grains (<50 μm) are also present in this stage. Finally, a late Zn–In–Cd bearing stage (Ps_3) has been recognized at a microscopic scale. It is characterized by a delicate interlayering of botryoidal bands of Fe-poor sphalerite and greenockite–hawleyite (Crespi et al., 2006), followed by tiny (<25 μm) idiomorphic crystals of greenockite–hawleyite (Jovic et al., 2011a).

The indium concentrations in the polymetallic veins show a wide variation, from 3.4 to 1184 ppm. The highest indium content is related to the Ps_2 mineralization stage, although significant In contents (up to 159 ppm) are also present in the Ps_1 paragenesis. Three types of In associations were distinguished on the basis of ore micro-analytical studies (Jovic et al., 2011c). The Fe-rich sphalerite in Ps_2, volumetrically important at this stage, has very high In contents (up to 2.56 wt.% In), and is therefore considered to be the most important In carrier. Tin minerals (ferrokësterite and cassiterite) in the Ps_1 assemblage are second in importance, with contents reaching up to 3.02 wt.%. The third In association type is represented by greenockite–hawleyite crystals (assemblage Ps_3), with high In contents (up to 3.63 wt.%), but these minerals are volumetrically negligible within the deposit.

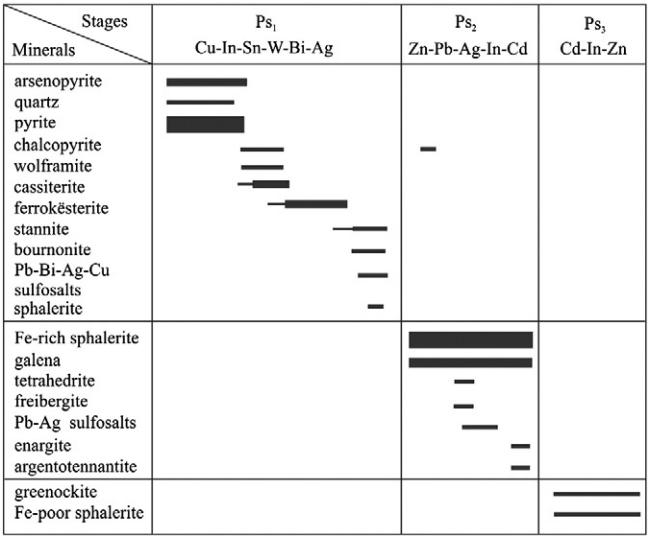

Fig. 4. Paragenetic diagram for the sulfide veins at the Pingüino deposit showing polymetallic stage 1 (Ps_1), polymetallic stage 2 (Ps_2) and polymetallic stage 3 (Ps_3).

Hydrothermal overprint associated with the mineralization is characterized by advanced argillic alteration within the immediate vein zone, and a wide envelope of sericitic alteration around the vein zone. Fluid inclusion studies indicate homogenization temperatures of 308–327° for Ps_1 (quartz) and 255–312.4° for Ps_2 (sphalerite), and low to moderate salinities (2 to 5 eq. wt.% NaCl and 4 to 9 eq. wt.% NaCl, respectively) (Jovic et al., 2011a). The isotopic $\delta^{34}S$ CDT values of sulfide minerals (+0.76 to +3.61‰) indicate a possible magmatic source for the sulfur in the polymetallic mineralization, whereas the Pb isotope ratios for the sulfides and magmatic rocks ($^{206}Pb/^{204}Pb = 17.379 = 18.502$; $^{207}Pb/^{204}Pb = 15.588–15.730$; $^{208}Pb/^{204}Pb = 38.234–38.756$) are consistent with the possibility that both derived from the same crustal Pb source (Jovic et al., 2011a). The spatial relationships, hydrothermal alteration styles, S and Pb isotopic data suggest a probable genetic link between the polymetallic mineralization and the dioritic intrusions which could have been the source for the metals and hydrothermal fluids (Jovic et al., 2011a).

4. Indium geochemistry

4.1. Methodology

In order to determine the metal distributions at the deposit scale, statistical analysis of the geochemical data from drill-core and trench samples was performed. Samples from 422 diamond drill cores, 225 reverse circulation drill cores (RC) and 551 trenches were examined and more than >50,000 samples were analyzed by inductively-coupled-plasma mass-spectrometry (ICP-MS). From this database, only vein samples were selected for further analysis. To perform this selection, each sample was identified as vein mineralization, disseminated mineralization or stockwork halo, or a host rock according to geological logs and cross-section interpretation. The size of mineralized samples varies between 0.4 and 1 m long. For more widely distributed mineralization, several one-meter samples were examined. Samples from RC were taken from each meter of the drill hole and mineralization style was identified from geological logs.

Trench samples were 2 m long from barren part and <1 m long according to geological criteria; samples were obtained with a saw, hammers and chisels (Ristorcelli et al., 2013).

ICP-MS analyses were performed at the Acme Analytical Laboratories; trench and drill-core samples were analyzed for Au using fire assay with an atomic absorption (AA) finish (Acme 6 FA procedure) or with a gravimetric finish and for Au and other elements using the ICP-MS 1DX (including In and Sn) procedure. Samples with low silver contents were analyzed by aqua regia digestion with an AA finish; for silver contents over 50 ppm, analysis was by fusion together with the Au and gravimetric measurements. For the fire assay determination of Au, the sample was heated with $AgNO_3$ to 1050°; then HNO_3 and HCl were aggregated and put in a microwave; once cool, the measurement was taken with water. In the 1DX routine, sample splits of 0.5 g were leached in 95 °C aqua regia and analyzed by ICP-MS for the following elements: Ag, Al, As, Au, B, Ba, Bi, Ca, Cd, Co, Cr, Cu, Fe, Ga, Hg, In, K, La, Mg, Mn, Mo, Na, Ni, P, Pb, S, Sb, Sc, Se, Sn, Sr, Th, Ti, Tl, U, V, W and Zn. Only the data for Ag, Au, Cd, Cu, In, Sn, Pb, and Zn are incorporated in the present report. Samples with Zn, Pb, Ag and/or Cu contents above their upper detection limit re-analyzation using the ore-grade high-detection-limit 7AR procedure employing inductively-coupled-plasma emission spectrometry (ICP-ES). Samples with Ag contents exceeding the limit of detection by ICP-ES

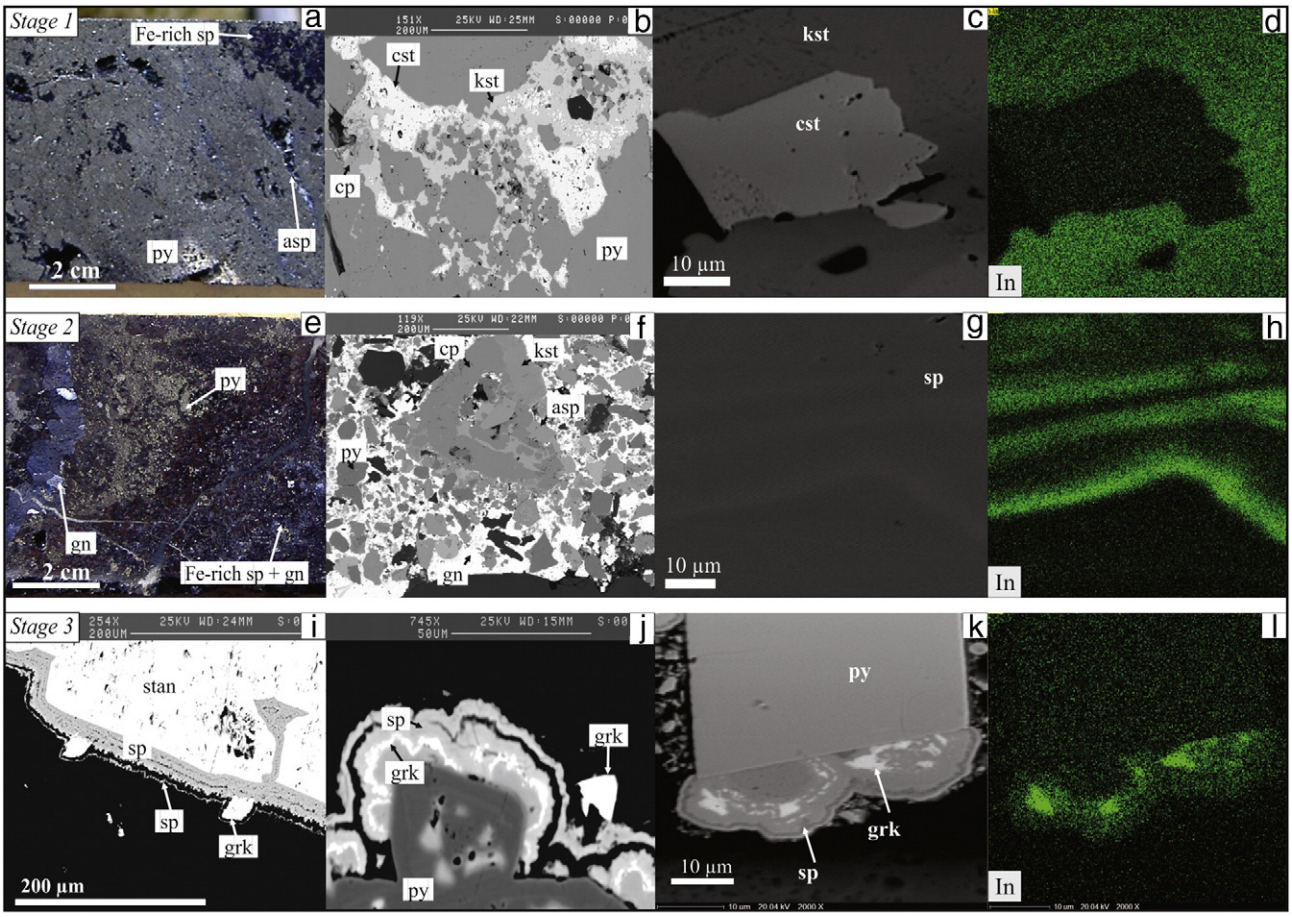

Fig. 5. a–d) Representative sample of stage Ps_1 polymetallic ore: a) pyrite (py) and arsenopyrite (apy) cross-cut by Fe-rich sphalerite (sp); b) back-scattered electron (BSE) image showing pyrite (py) and chalcopyrite (cp) crystals brecciated and healed by cassiterite (cst) and ferrokësterite (fks); c) BSE image of ferrokësterite (fks) and cassiterite (cst) crystals; d) In distribution map. e–h) Representative sample of stage Ps_2 ore: e) banded Fe-rich sphalerite (sp) and galena (gn) breccia with pyrite (py) clasts; f) BSE image of galena (gn) breccia with pyrite (py), chalcopyrite (cp) and ferrokësterite (fks) clasts; g) BSE image of banded Fe-rich sphalerite (sp) crystal; h) In distribution map. i–l) Representative sample of stage Ps3 ore: i) BES image of stannite (stan) and idiomorphic greenockite–hawleyite (grk) crystals surrounded by botryoidal banded Fe-poor sphalerite (sp); j) BSE image of botryoidal banded aggregate of greenockite–hawleyite (grk) encrusting a Fe-poor sphalerite (sp) and pyrite (py) crystal; k) BSE image of botryoidal banded aggregate of greenockite–hawleyite (grk) and Fe-poor sphalerite (sp) encrusting a pyrite (py) crystal; l) In distribution map.

and Au values exceeding 300 ppb were rerun using the G6 fire assay procedure (Ristorcelli et al., 2013).

These geochemical data were used to calculate the mean element content, standard deviation value and maximum content for each of the 19 veins studied in the present work (Table 1). These geostatistical data were mapped to evaluate the distribution of In and other metals.

Microprobe analysis of ore minerals in polished sections was performed and carried out at the Serveis CientíficoTècnics, Universitat de Barcelona, Spain, with a Cameca SX50 electron microprobe equipped with four wavelength-dispersive spectrometers and an energy-dispersive spectrometer. The analyses are presented elsewhere (Jovic et al., 2011c), and in the present work were used only to constrain variations in ore mineralogy.

Table 1
Mean values of selected element from mineralized samples of El Pingüino veins: MC (Marta Centro), ME (Marta Este), TR (Tranquilo), MN (Marta Norte), LUN (Luna), KAS (Kasia), MNW (Marta Noroeste), IVO (Ivonne), MS (Marta Sur), SON (Sonia), IVS (Ivonne Sur), CSV (Colita de Savary), SAV (Savary), IVN (Ivonne Norte), KAL (Kalia), KAR (Karina), ISL (Isla), MW (Marta Oeste), and FAN (Fantasma).

Ivonne Sur	159	15.4	0.3	17.0	449	4182	10,209	7.3
CSV	157	2.8	0.2	55.1	88	4831	4530	19.6
Savary	147	18.7	1.3	65.4	239	8785	10,030	6.2
Ivonne Norte	124	23.6	1.4	39.2	1702	1912	6024	4.4
Kalia	91	1.7	0.0	14.8	105	6612	6542	22.8
Karina	86	1.8	0.3	50.9	118	4124	339	14.3
Isla	69	0.0	0.8	28.0	38	55	221	5.9
Marta Oeste	49	6.5	0.3	36.3	72	4125	5299	3.5
Fantasma	33	0.0	0.2	51.1	51	584	262	7.0

4.2. Geochemical distribution

The distribution of metals at the Pingüino deposit displays a concentric pattern (Fig. 6), with the highest contents located in the central area of the deposit, mainly related to the Marta Centro, Marta Este, Ivonne Norte and Savary veins. Gold and Ag show a tendency to have the highest values in the central and northwestern areas of the deposit (Figs. 6a, b), whereas Cu and Pb are concentrated significantly in the central area, but also show high values in the northwestern and southeastern areas of the deposit (Figs. 6c, d).

Indium and Zn exhibit a similar distribution, and are very restricted to the central and southeastern areas (Figs. 6c, d). The In contents are very variable in the Pingüino veins and the highest mean contents are located toward the central area of the deposit. The Marta Centro vein exhibits the maximum mean In values of 34.8 ppm, whereas other veins with high values are: Ivonne Norte (23.6 ppm), Savary (18.7 ppm), Ivonne (17.6 ppm), Ivonne Sur (15.4 ppm) and Kasia (13.2 ppm). The In

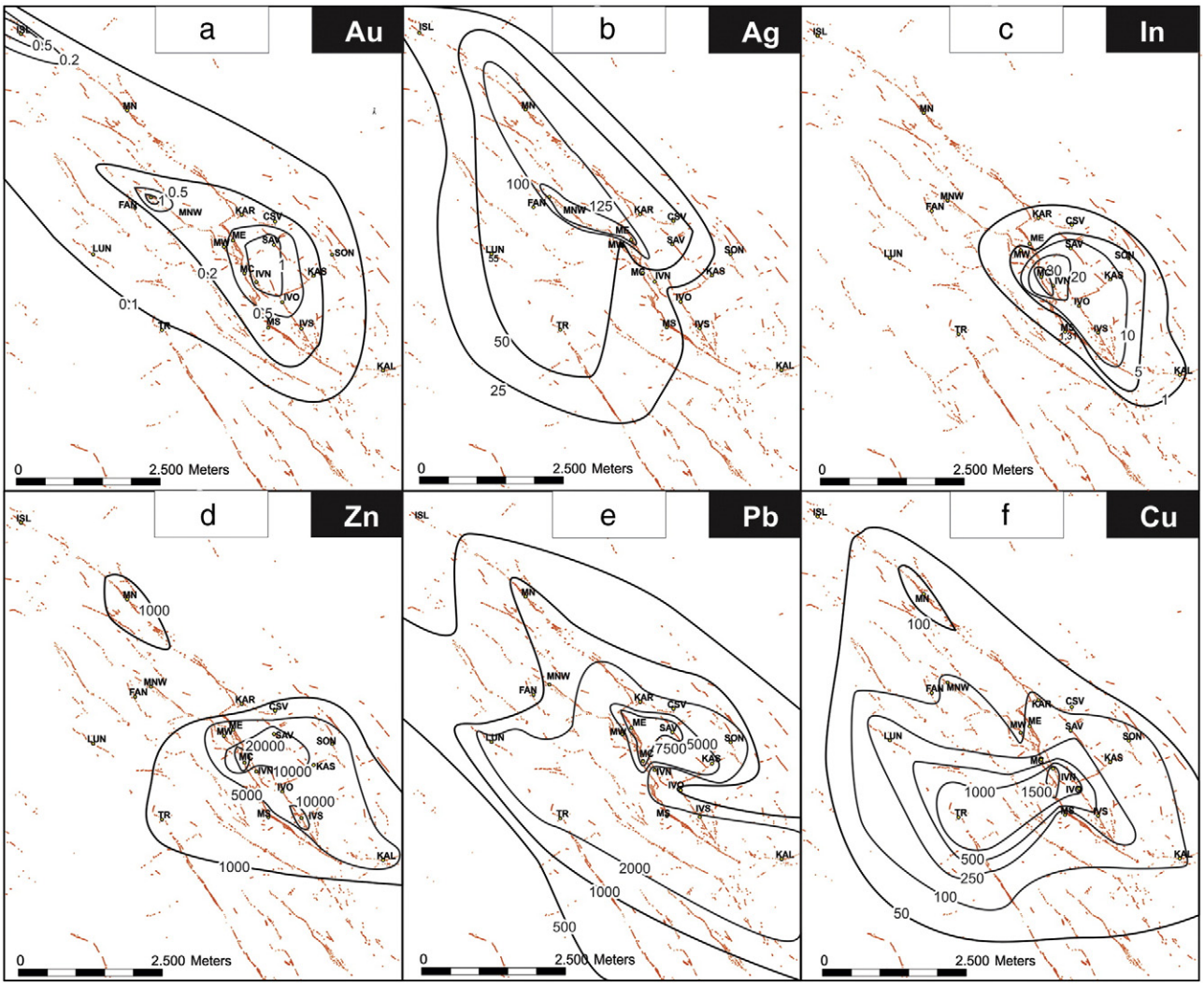

Fig. 6. Mean metal content maps of the Pingüino veins: a) gold, b) silver, c) indium, d) zinc, e) lead, and f) cooper.

distribution shows that the maximum values are located specifically in the Marta Centro and Ivonne Norte veins and extend further to the SSE through Ivonne and Ivonne Sur veins and to the ENE to Kasia and Savary veins. Fig. 7 shows an overlay of the In distribution map with the detailed magnetometry survey map for the deposit, from which a clear spatial relation between the localized concentration of In and the interpreted Kasia segmented intrusion (Fig. 3) can be seen, with the highest In values located immediately on the northern border of the Central-Kasia (Marta Centro–Ivonne Norte veins) and East-Kasia (Savary and Kasia veins) intrusions and between the two intrusions (Ivonne and Ivonne Sur veins).

4.3. Supergene behavior

The supergene weathering profile at the Pingüino deposit is relatively thin, ranging from 30 m to 80 m in thickness, and reaching maximum depths near Marta Este and Marta Noroeste. The thickness of the weathered profile can be readily correlated with a lithological contact between the tuffites of the Roca Blanca Formation and the mudstones and sandstone of the El Tranquilo Group, where the siltstones and shales acted as an impermeable layer, preventing oxidation from developing at lower levels.

To study the behavior of In in the supergene profile, 1700 geochemical samples from a total number of 108 holes and trenches were used. The depth of each sample is presented as meters below the surface, and the geochemical values are corrected for the sample length. The In behavior was compared with those of In-related elements like Zn, Cd and Sn and other elements, in the polymetallic veins, such as Cu and Pb. Vertical concentrations of In, Zn and Pb are presented in a typical cross-section of the In-rich Marta Centro vein in Figs. 8 and 9.

Lead exhibits a fairly uniform distribution unaffected by oxidation; this pattern is consistent with the conventional interpretation of the geochemical behavior of Pb, which is considered to be a very immobile element within the oxidized zone (Figs. 8a and 9d). The Cu content is fairly low; however, a distinct increase in Cu values around 50 m below the surface is observed and probably related to secondary enrichment processes (Fig. 8b).

Variations in Zn content with depth (Figs. 8c and 9c), reveal relatively constant Zn values in the primary zone and a dramatic decrease in the concentration of this metal near and above the oxidation limit in accord with the geochemical behavior of Zn, which is typically very mobile in the oxidized zone. A similar behavior was observed for Cd, with an important decrease of its concentration across the oxidation zone (Fig. 8d). Tin distribution, on the other hand, is quite uniform vertically and shows a behavior similar to that of Pb (Fig. 8e).

The In concentrations show a near-constantly uniform pattern with minor variations and remain virtually constant across the oxidation zone. Even in surface trenches, where values exceeding 100 ppm were observed, In shows a behavior similar to that of Pb and Sn, which implies that it also behaved as an immobile element (Figs. 8f and 9b).

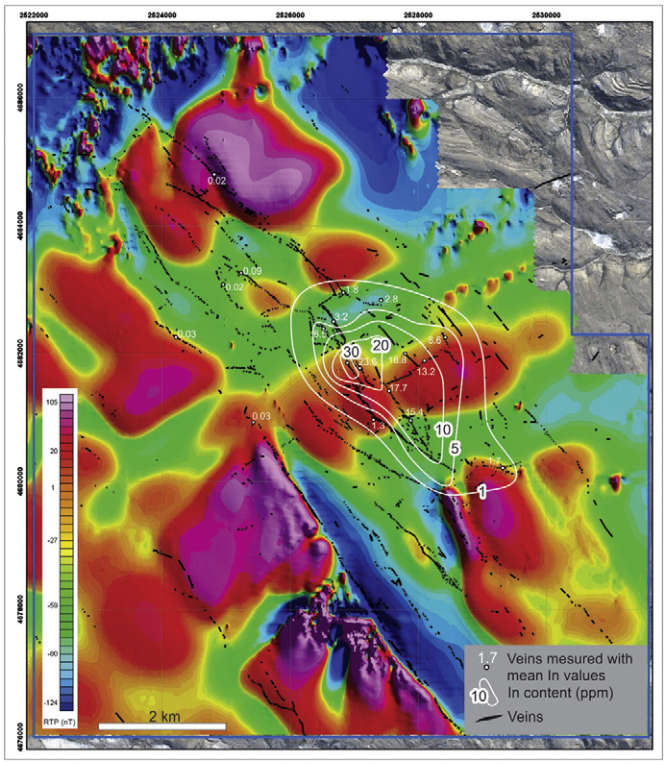

Fig. 7. In content map of the Pingüino veins superimposed on a detailed magnetometry (RTP) map of the area. Dashed lines mark unexposed intrusion. Veins' abbreviations as in Fig. 2a.

5. Discussion

The In-bearing polymetallic vein-type ore deposits are a very heterogeneous group, showing transitions to granite-related vein-stockwork and porphyry Sn–W deposits and to base metal-rich epithermal-style mineralization (Schwarz-Schampera and Herzig, 2002). Most of these deposits are structurally controlled and occur in faults and fault systems genetically linked with magmatic activity, mainly represented by intermediate to felsic subvolcanic intrusions. Mineralizing fluids display evidence for heterogeneous source showing variable degrees of mixing between high-temperature magmatic fluids and meteoric waters, and formation temperatures ranging from 250° to 380° (Ohta, 1995; Schwarz-Schampera and Herzig, 2002).

Only a few In minerals are known in nature (Schwarz-Schampera and Herzig, 2002). Roquesite ($CuInS_2$) is the most common In mineral and has been identified worldwide at several localities (Cook et al., 2011b). Where there is an excess of Zn in the system, sphalerite is the preferred host for In, and roquesite is not formed under these conditions (Cook et al., 2011a). Indium is incorporated in sphalerite in accord with the substitution $(Cu^{+},In^{+3}) \leftrightarrow (Zn^{+2},Fe^{+2})$ (Cook et al., 2009, 2011a,b, 2012). In addition, stannite (kësterite), stannoidite and casiterite have been mentioned as hosts for In (Cook et al., 2011a,b).

5.1. Behavior of indium in hydrothermal solutions

Despite the importance of hydrothermal processes in generating In-bearing ores, very little is known about the aqueous geochemistry of this element, especially at elevated temperatures and pressures. In particular, solubility of relevant minerals, and stabilities of aqueous complexes containing In at conditions relevant to hydrothermal and supergene ore formation have received relatively little attention (Wood and Samson, 2006).

The dioritic subvolcanic intrusions were probably the source of metals for the Pingüino deposit, where hydrothermal fluids, mixed with meteoric waters, depositioned in the In-bearing polymetallic mineralization (Jovic, 2010; Jovic et al., 2011a). At the deposit scale, the higher In contents show a clear spatial relation with the Kasia segmented intrusion (of probable dioritic composition), being the specific main source of the hydrothermal fluids. These fluids were channeled, mainly by NNW fractures (Tranquilo trend), to move to the SSE with a secondary trend to the ENE (Kasia trend), indicating that both channel systems were active during the polymetallic ore deposition, while in the NW-oriented

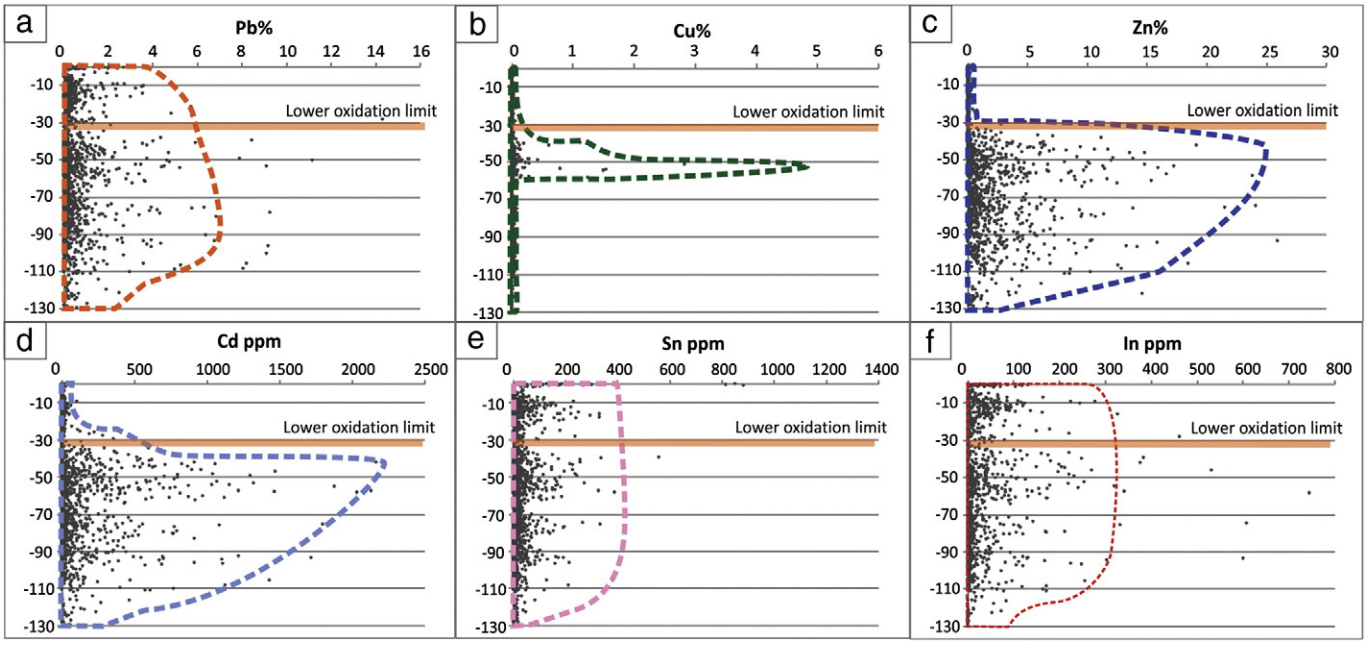

Fig. 8. Surface element distribution patterns corrected for length vs. deep for the Marta Centro vein (see Fig. 2a for location). Dotted lines delineate the maximum density of data points. a) Pb pattern showing fairly consistent concentration values regardless of depth. b) Copper distribution showing a secondary enrichment zone at a depth of ~50 m. c, d) Zinc and Cd patterns, respectively, showing a drastic decrease in concentration values close to the oxidation zone. e, f) Tin and In patterns, respectively showing consistent metal concentrations regardless of the position relative to the oxidized zone.

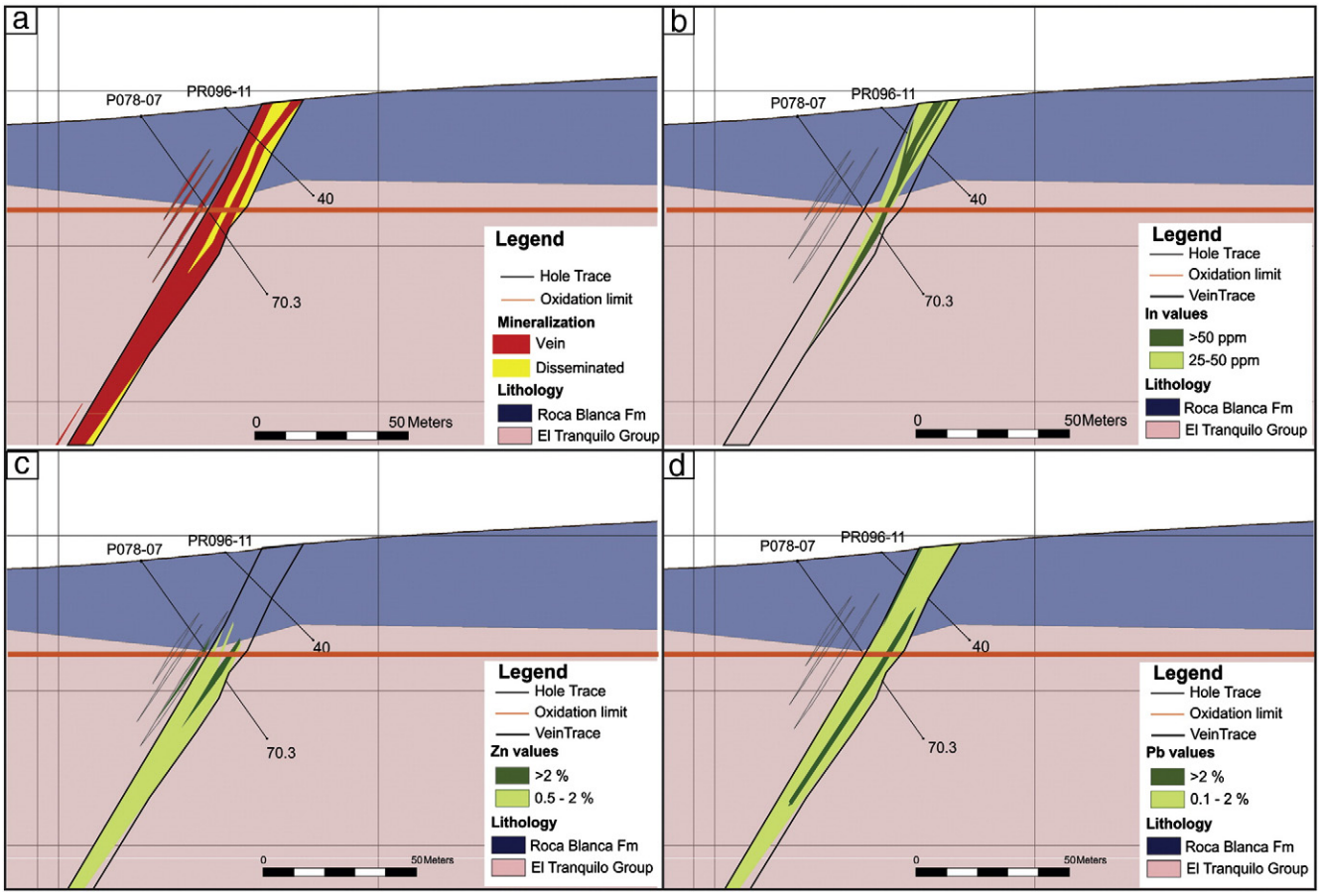

Fig. 9. Marta Centro vein (see Fig. 2a for location). a) Relative position of vein and disseminated mineralization. b) Indium distribution along the vein. c) Zinc distribution along the vein; note a decrease in Zn values at the oxidation limit. d) Lead distribution, shows nearly consistent Pb values along the vein.

fractures (Marta trend), no polymetallic veins were found. Hence we interpret the Marta trend as a later-developed fracture system related to the late Ag–Au quartz-rich veins.

At the vein scale, the hypogene distribution of In seems to have been controlled by deposition temperatures. In the Ps_1 assemblage, In is hosted in ferrokësterite and cassiterite (Crespi et al., 2006; Jovic et al., 2011c) with formation temperatures between 308 and 327 °C, while in the Ps_2 assemblage, sphalerite is the main In-carrier with formation temperatures between 255 and 312 °C (Jovic et al., 2011a).

5.2. Supergene behavior of indium

There is only scarce information on the solubility of aqueous solutions (e.g., Wood and Samson, 2006) and its geochemical behavior under supergene conditions. The stability of In in the supergene zone could be related to the extremely low solubility of this element at pH values between ~4.5 and ~9, and in the temperature range of supergene conditions (Ogawa et al., 2012; Schwarz-Schampera and Herzig, 2002), which is supported by the precipitation of In as hydroxide during experimental studies at these conditions (Wood and Samson, 2006). Dzhalindite [$In(OH)_3$] has been reported from this type of environment at several Zn and Sn deposits (e.g., Dill et al., 2013).

At the Pingüino deposit, the vertical distribution shows a near constant concentration independent of the depth. No clear departure of In values from that typical range was observed below or above the oxidation level, which is similar to the distribution pattern of Pb and Sn (Fig. 8). This could imply that In behaved as an immobile element in the supergene zone. This behavior is undoubtedly linked to the low mobility of this metal under moderate pH conditions prevalent in the oxidized zone (Wood and Samson, 2006).

6. Conclusions

1) The In-bearing polymetallic mineralization at Pingüino is spatially and genetically related to the Lower Jurassic dioritic intrusions, particularly the ENE-trending unexposed Kasia intrusions. These intrusions are considered the principal source of hydrothermal fluids responsible for the deposition of the In-bearing mineralization. The fluids were channeled mainly by NNW-trending fractures (Tranquilo trend), with a second-order distribution following the ENE Kasia trend, suggesting that both were active during the polymetallic ore deposition.
2) At the vein scale, the hypogene In distribution was controlled mostly by fluid temperatures. In the Ps_1 stage, indium was incorporated in ferrokësterite and cassiterite (T = 308–327 °C); while in the Ps_2 stage, sphalerite was the main In-carrier (T = 255–312 °C).
3) The vertical distribution of In at Pingüino shows little variation in concentration with depth. No clear correlation was observed between the In values and proximity to the oxidation level. Indium is interpreted to exhibit a behavior similar to that of Pb and Sn, which implies that this metal is immobile during weathering of polymetallic ores.

Acknowledgments

The authors want to thank Mariano Mongan, Mike Brown and the Argentex Mining Corporation staff for their help, discussions and access to their data, and Ramiro Lenarduzzi for his assistance with the geochemical database. Nigel Cook and Krister Sundblad are thanked for their very constructive reviews. We also would like to thank Anton

R. Chakhmouradian, Jindrich Kynicky and Martin Smith for their editorial help and the invitation to contribute to this special issue.

References

Cook, N.J., Ciobanu, C.L., Pring, A., Skinner, W., Shimizu, M., Danyushevsky, L., Saini-Eidukat, B., Melcher, F., 2009. Trace and minor elements in sphalerite: a LA-ICPMS study. Geochim. Cosmochim. Acta 73, 4761–4791.

Cook, N.J., Ciobanu, C.L., Williams, T., 2011a. The mineralogy and mineral chemistry of indium in sulphide deposits and implications for mineral processing. Hydrometallurgy 108, 226–228.

Cook, N.J., Sundblad, K., Valkama, M., Nygård, R., Ciobanu, C.L., Danyushevsky, L., 2011b. Indium mineralisation in A-type granites in southeastern Finland: insights into mineralogy and partitioning between coexisting minerals. Chem. Geol. 284, 62–73.

Cook, N.J., Ciobanu, C.l., Brugger, J., Etschmann, B., Howard, D. l, De jonge, M. d, Ryan, C., Paterson, D., 2012. Determination of the oxidation state of Cu in substituted Cu–In–Fe-bearing sphalerite via m-XANES spectroscopy. Am. Mineral. 97, 476–479.

Cortiñas, J., Homovc, J., Lucero, M., Gobbo, E., Laffitte, G., Viera, A., 2005. Las cuencas de la región del Deseado, provincia de Santa Cruz. Frontera exploratoria de la argentinaInstituto Argentino del Petróleo y del Gas, Buenos Aires, pp. 289–305.

Crespi, A., Jovic, S., Guido, D., Proenza, J., Melgarejo, J.C., Schalamuk, A., 2006. El prospecto Cerro León, Macizo del Deseado, Patagonia, Argentina: Un depósito de Ag–Sn. Rev. Macla. 6, 143–145.

Dill, H.G., Garrido, M.M., Melcher, F., Gomez, M.C., Weber, B., Luna, L.I., Bahr, A., 2013. Sulfidic and non-sulfidic indium mineralization of the epithermal Au–Cu–Zn–Pb–Ag deposit San Roque (Provincia Rio Negro, SE Argentina) – with special reference to the “indium window” in zinc sulfide. Ore Geol. Rev. 51, 103–128.

Echavarría, L.E., Schalamuk, I.B., Etcheverry, R.O., 2005. Geologic and tectonic setting of Deseado Massif epithermal deposits, Argentina, based on El Dorado-Monserrat. J. S. Am. Earth Sci. 19, 415–432.

Fernández, R.R., Blesa, A., Moreira, P., Echeveste, H., Mykietiuk, K., Andrada de Palomera, P., Tessone, M., 2008. Los depósitos de oro y plata vinculados al magmatismo jurásico de la Patagonia: revisión y perspectivas para la exploración. Rev. Asoc. Geol. Argent. 665–681.

Gómez, C., Luna, L., Garrido, M., Bonuccelli, R., 2008. Manifestación de indio en el Macizo Nordpatagónico: proyecto San Roque, provincia de Rio Negro. 9° Congreso de Mineralogía y Metalogenia, pp. 125–128.

González Guillot, M., De Barrio, R., Ganem, F., 2004. Mina Martha, un yacimiento epitermal argentífero en el Macizo del Deseado, provincia de Santa Cruz. VII Congreso de Mineralogía y Metalogenia, pp. 119–204.

Gozalvez, M., Herrmann, C., Segal, S., Crosta, S., Romano, A., 2008. Avances en el conocimiento de la mineralización del depósito Gonzalito, provincia de Rio Negro, Argentina. 9° Congreso de Mineralogía y Metalogenia, pp. 129–132.

Guido, D., Schalamuk, I., 2003. Genesis and exploration potential of epithermal deposits from the Deseado Massif, Argentinean Patagonia. Miner. Explor. Sustain. Dev., vol. I. Balkema-Rotterdam, pp. 493–496.

Guido, D.M., Jovic, S.M., Schalamuk, I.B., 2005. A new metallogenic association (Sn–Cd–In–Zn–Ag–Au) in the Deseado Auroargentiferous province, Deseado Massif, Patagonia, Argentina. Meeting the Global Challenge — 8th SGA Meeting, Beijing, China. Miner. Dep. Res., 2, pp. 965–968.

Herbst, R., 1965. La flora fósil de la Formación Roca Blanca, provincial de Santa Cruz, Patagonia, con consideraciones geológicas y estratigráficas. Opera Lilloana 12, 1–102.

Jalfin, G., Herbst, R., 1995. La Flora triásica del Grupo El Tranquilo, provincia de Santa Cruz (Patagonia). Estratigrafía, 32(3). Ameghiniana, pp. 211–229.

Jovic, S., 2010. Geología y Metalogénesis de las mineralizaciones polimetálicas del área El Tranquilo (Cerro León), sector central del Macizo del Deseado, Provincia de Santa Cruz, 1ra ed. Editorial de la Universidad de La Plata (EDULP), La Plata, (278 pp.).

Jovic, S.M., Guido, D.M., Schalamuk, I.B., Ríos, F.J., Tassinari, C.C.G., Recio, C., 2011a. Pingüino in-bearing polymetallic vein deposit, Deseado Massif, Patagonia, Argentina: characteristics of mineralization and ore-forming fluids. Miner. Depos. 46, 257–271.

Jovic, S.M., Guido, D.M., Ruiz, R., Páez, G.N., Schalamuk, I.B., 2011b. Indium distribution and correlations in polymetallic veins from Pingüino deposit, Deseado Massif, Patagonia, Argentina. Geochem. Explor. Environ. Anal. 11, 107–115.

Jovic, S.M., Guido, D.M., Melgarejo, J.C., Páez, G.N., Ruiz, R., Schalamuk, I.B., 2011c. The indium-bearing minerals of the Pingüino polymetallic vein system, Deseado Massif, Patagonia, Argentina. Can. Mineral. 49, 931–946.

Marifil Mines Ltd., 2010. Toruel Project Rio Negro Province. NI 43-101 Technical ReportMarifil Mines Ltd., Argentina, http://www.marifilmines.com.

Murakami, H., Ishihara, S., 2013. Trace elements of Indium-bearing sphalerite from tin-polymetallic deposits in Bolivia, China and Japan: a femto-second LA-ICPMS study. Ore Geol. Rev. 53, 223–243.

Ogawa, Y., Ishiyama, D., Shikazono, N., Iwane, K., Kajiwara, M., Tsuchiya, N., 2012. The role of hydrous ferric oxide precipitation in the fractionation of arsenic, gallium, and indium during the neutralization of acidic hot spring water by river water in the Tama River watershed, Japan. Geochim. Cosmochim. Acta 86, 367–383.

Ohta, E., 1995. Common features and genesis of tin-polymetallic veins. Resour. Geol. Spec. Issue 18, 187–195.

Páez, G.N., Ruiz, R., Guido, D.M., Jovic, S.M., Schalamuk, I.B., 2011. Structurally controlled fluid flow: high-grade silver ore-shoots at Martha epithermal mine, Deseado Massif, Argentina. J. Struct. Geol. 33, 985–999.

Pankhurst, R., Leat, P., Sruoga, P., Rapela, C., Márquez, M., Storey, B., Riley, T., 1998. The Chon Aike province of Patagonia and related rocks in West Antarctica: a silicic large igneous province. J. Volcanol. Geotherm. Res. 81, 113–136.

Panza, J., 1995. Hoja geológica 4969-II Tres Cerros escala 1: 250.000, Provincia de Santa Cruz. Dirección Nacional del Servicio Geológico Boletín. 213, 103 pp.

Peñalva, G.A., Jovic, S.M., Chernicoff, C.J., Guido, D.M., Schalamuk, I.B., 2008. Cuerpos intrusivos asociados a las mineralizaciones polimetálicas del depósito Cerro León, área del anticlinal El Tranquilo, Santa Cruz: Evidencias Geofísicas. Rev. Asoc. Geol. Argent. 63 (1), 14–23.

Ristorcelli, S., Ronning, P., Tucker, R., Guido, D., 2013. Technical Report on the Pingüino Project Santa Cruz Province, Argentina (143 pp.).

Schalamuk, I., de Barrio, R., Zubia, M., Genini, A., Echeveste, H., 1999. Provincia Auroargentífera del Deseado, Santa Cruz. Recursos Minerales de la República Argentina. Instituto de Geología y Recursos Minerales, 35. SEGEMAR, pp. 1177–1188.

Schwarz-Schampera, U., Herzig, P.M., 2002. Indium. Geology, Mineralogy, and EconomicsSpringer, Berlin, (257 pp.).

Trendix, S.A., 2006. http://www.trendixmining.com.ar.

Wood, S.A., Samson, I.M., 2006. The aqueous geochemistry of gallium, germanium, indium and scandium. Ore Geol. Rev. 28, 57–102.